

## STATISTICAL ANALYSIS OF THE EDGE FLAME PROPAGATION IN A TURBULENT LIFTED FLAME

**Shahram Karami**

School of Photovoltaic and Renewable  
Energy Engineering,  
The University of New South Wales,  
Sydney, 2052 AUSTRALIA,  
s.karami@unsw.edu.au

**Mohsen Talei**

Department of Mechanical Engineering,  
The University of Melbourne,  
Melbourne, 3010 AUSTRALIA,  
mohsen.talei@unimelb.edu.au

**Evatt R. Hawkes**

School of Photovoltaic and Renewable Energy Engineering  
/ School of Mechanical and Manufacturing Engineering,  
The University of New South Wales,  
Sydney, 2052 AUSTRALIA,  
evatt.hawkes@unsw.edu.au

### ABSTRACT

This paper presents a statistical analysis of edge flames in a turbulent lifted flame using direct numerical simulation (DNS). To investigate the dynamics of edge flames, a theoretical framework describing the edge-flame propagation velocity as a function of propagation velocities of mixture fraction and product mass fraction iso-surfaces at the flame base is used. The correlations between these propagation velocities and scalar dissipation rate, orientations and gradients of product mass fraction and mixture fraction are then studied.

The analysis reveals that negative edge-flame velocity, which may be interpreted as an extinction, occurs at high scalar dissipation rate. The responses of propagation velocities to scalar dissipation are explained using the correlation of contributing terms, namely the reaction, tangential and normal diffusions terms and using the statistics of alignment between product mass fraction and mixture fraction gradients.

### Introduction

Lifted flames are well-known configurations commonly have been observed in industrial burners, gas turbines and diesel engines. They occur when the jet velocity is high enough to prevent flames being anchored at the nozzle lip. The location of the flame base has important implications for the design of the burners and the emissions that they produce. As a result, a vast body of literature exists on understanding how lifted flames are stabilised (Stårner *et al.*, 1996; Arndt *et al.*, 2013; Su *et al.*, 2006). Nevertheless, the stabilisation mechanism is still a poorly understood phenomenon and there has been a limited concord among the researchers regarding the dominant stabilisation mechanism. In laminar lifted flames, which are rarely encountered in industrial applications, it is believed that a partially premixed, self-propagating edge-flame (also known as triple-flame or tribrachial-flame) that is centred at vicinity of the stoichiometric mixture fraction surface is the main stabilisation mechanism (Ghosal & Vervisch, 2000; Chung, 2007). In the presence of low strain rates, the edge-flame structure consists of two wings of premixed flames

and a tail of a non-premixed (diffusion) flame. However, when the edge-flame experiences high strain rates, one or both premixed branches collapse on the non-premixed tail creating a comet-shape structure. The edge flame was first experimentally reported by Phillips (1965) showing that a self-propagating edge flame was present in the interface between a layer of methane and air.

However, the situation is more complicated in turbulent lifted flames. A number of theories such as the premixed flame theory, the edge-flame theory, the critical dissipation rate theory, and several theories involving a role played by large eddies have been proposed in the literature. However, there is not a single theory that can generally describe the stabilisation mechanism in turbulent lifted flames. Among these theories, it was found in our previous study (Karami *et al.*, 2014) that the combination of the edge-flame and large-eddy theories can explain the stabilisation mechanism in low lifted height flames.

A close review of the literature shows that the dynamics of edge-flame structure in turbulent flames have been relatively less studied. This structure has been reported in several experimental studies of turbulent lifted flames (Stårner *et al.*, 1996; Arndt *et al.*, 2013). However, measuring the parameters of interest is extremely challenging in experiment (Gordon *et al.*, 2012; Upatnieks *et al.*, 2004). As a result, the experimental studies are not able to provide a comprehensive picture on the stabilisation process.

Direct numerical simulation (DNS) is a powerful tool that can provide a detailed understanding about the effect of important parameters on the edge-flame structure. However, due to its high computational cost, DNS studies of edge flames in a turbulent jet have been limited to very few in the literature (Pantano, 2004; Karami *et al.*, 2012, 2014). Pantano (2004) used DNS with reduced chemistry to study non-premixed flame extinction in a methane-air jet flame. He developed a theoretical framework in which the edge-flame propagation was described as a function of the propagation velocities of the mixture fraction and a scalar iso-surfaces and their alignment. His analysis of the resulting edge propagation velocity showed that this velocity is

largely controlled by the local rate of scalar dissipation.

In our DNS study (Karami *et al.*, 2014), it was shown that the flow on average balances the relative propagation of the edge-flame supporting the edge-flame stabilisation theory. Conditioning of the net flame velocity on stream-wise and transverse location revealed an elliptical clockwise motion of the edge-flames around the average stabilisation point. Mostly as consistent with observation of Su *et al.* (2006), it was proposed that this motion is connected with the passage of large eddies. However, it was suggested that an out-of-plane motion around large eddies plays a role in the stabilisation process. These studies revealed some features of the edge-flame structure. However, the effects of scalar dissipation, scalar gradients and orientations on the edge-propagation velocity have not been addressed in the literature yet.

The aim of this paper is therefore to address this gap by providing an analysis of the effect of important parameters on the edge-flame dynamics using DNS (Karami *et al.*, 2014, 2015). These parameters include displacement speeds of the product mass fraction and mixture fraction iso-surfaces, the orientations of the normal vectors to these iso-surfaces, scalar dissipation rate and gradients of product mass fraction and mixture fraction. The curvatures of product mass fraction and mixture fraction and strain rates on mixture fraction and product mass fraction also important which will be discussed in a more comprehensive paper which is under preparation (Karami *et al.*, 2015).

## COMPUTATIONAL APPROACH

The configuration of a slot jet flame similar to that studied in Yoo *et al.* (2009) is used. The conservation equations of mass, momentum, sensible energy and fuel and oxidiser mass fraction are nondimensionalised with respect to the inlet jet width,  $H$ , the speed of sound, temperature and thermodynamic properties on the jet centreline at the inlet. A single-step chemistry is used for the chemistry model. To capture the laminar flame propagation speed of methane-air reaction, the modified activation energy approach by Garrido-López & Sarkar (2005), where the same function proposed by Fernández-Tarrazo *et al.* (2006) for activation energy is used. These equations are solved in a non-dimensional form employing the DNS code S3D\_SC (Karami *et al.*, 2012, 2014, 2015). S3D\_SC is a modified version of the detailed chemistry code S3D (Chen *et al.*, 2009).

The mean inlet axial velocity and fuel mass fraction were specified using a tanh-based profile. The inlet normalized velocity of jet is 0.48 with a co-flow of 0.001 which implies a Reynolds number of 5,280 inlet. The inlet momentum (and mixing layer) thickness,  $\delta$ , is equal to  $0.05H$ . To describe the velocity fluctuations at the inlet,  $u$ , a homogeneous isotropic turbulence field based on a prescribed turbulent energy spectrum (Passot & Pouquet, 1987) with a turbulence intensity of 5% is first produced. These velocity fluctuations are then added to the mean inlet velocity using the Taylor's frozen turbulence hypothesis (Yoo *et al.*, 2009). The fuel stream is pure fuel while the co-flow is air with an air-fuel ratio of 4.0 and a stoichiometric mixture fraction of 0.055. The reader is referred to Karami *et al.* (2014) for more details of numerical schemes, boundary conditions, grid spacing and thermal-turbulence resolutions.

The simulation was run for 18.0 jet flow through times,  $t_j = L_x/U_j$  (where the  $L_x$  is the length of the computational domain in the streamwise direction), to obtain a statistically stationary solution and the data of the last  $12.0t_j$  were used

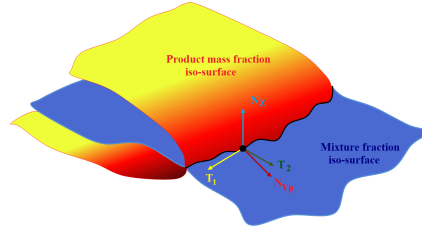


Figure 1: Various normal and tangential vectors at the flame base (the red surface is the product mass fraction iso-surface, the blue surface is the mixture-fraction iso-surface and the solid black line is the edge-flame).

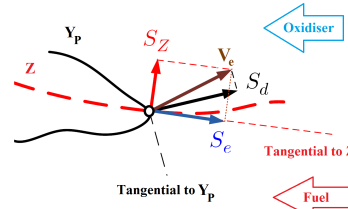


Figure 2: Schematic of edge-flame propagation along the mixture fraction iso-surface.

for the analysis.

## MATHEMATICAL BACKGROUND

Now some necessary background regarding the identification of edge-flames and their speeds relative to the flow will be developed in this section. Some of these materials are repeated from our earlier study (Karami *et al.*, 2014) for the sake of completeness.

In premixed combustion, flame speeds are frequently obtained by calculating the displacement speed of a reacting scalar at a location in the flame that approximately tracks the locations of peak heat release (Echehki & Chen, 1998; Im & Chen, 2001; Hawkes & Chen, 2006; Chakraborty & Cant, 2004). More detail of the numerical schemes can be found in Karami *et al.* (2014).

In partially premixed flames, the situation is more complicated. Observations from DNS (Pantano, 2004; Hawkes *et al.*, 2007; Karami *et al.*, 2014) show that the edge-flames tend to remain anchored near to a particular mixture-fraction iso-surface. Therefore, following earlier studies of extinction and reignition (Pantano, 2004; Hawkes *et al.*, 2007), and our previous study (Karami *et al.*, 2014), we select an edge-flame marker that is the intersection of a mixture-fraction iso-surface and a product mass-fraction iso-surface. A slightly rich mixture fraction of 0.07, corresponding to maximum laminar speed of 1D flame, and a product mass fraction of 0.2, corresponding to maximum reaction rate of a triple flame, were selected for these two iso-surfaces.

To analyse the edge flame motion, a coordinate system moving with the flow velocity is first defined – see figure 1. In the figure: the normal to the mixture-fraction iso-surface is denoted  $N_Z$  (pointing towards oxidiser); the normal to the product mass-fraction iso-surface is denoted  $N_{Y_p}$  (pointing towards reactants); the tangent to the mixture-fraction iso-surface which points along the flame edge is denoted  $T_1$ ; and finally, the tangent to the mixture-fraction iso-surface which is normal to  $T_1$ , and pointing towards the reactants is denoted  $T_2$ . It can be shown that these quantities are given

by:

$$\begin{aligned} \mathbf{N}_Z &= -\frac{\nabla Z}{|\nabla Z|}, \mathbf{N}_{Y_p} = -\frac{\nabla Y_p}{|\nabla Y_p|}, \\ \mathbf{T}_1 &= \frac{\mathbf{N}_{Y_p} \times \mathbf{N}_Z}{|\mathbf{N}_{Y_p} \times \mathbf{N}_Z|}, \mathbf{T}_2 = \frac{\mathbf{N}_Z \times (\mathbf{N}_{Y_p} \times \mathbf{N}_Z)}{|(\mathbf{N}_{Y_p} \times \mathbf{N}_Z)|}. \end{aligned} \quad (1)$$

Figure 2 shows a schematic, in the plane containing both  $\mathbf{N}_Z$  and  $\mathbf{N}_{Y_p}$ , of the edge-point motion. Because the chosen coordinate system moves with the local flow velocity, only the motion of the iso-surfaces relative to the flow need be considered. Relative motion is a result of relative displacement of both the mixture-fraction and the product mass-fraction iso-surfaces. The mixture-fraction iso-surface moves with the velocity of  $S_Z \mathbf{N}_Z$ , while the  $Y_p = Y_p^*$  iso-surface moves with the velocity of  $S_d \mathbf{N}_{Y_p}$ , where the displacement speeds are given as (Pope, 1988; Echekki & Chen, 1998)

$$\begin{aligned} S_Z &= \frac{1}{\rho |\nabla Z|} \left( -\frac{\partial}{\partial x_j} \left( \frac{\mu}{Sc} \frac{\partial Z}{\partial x_j} \right) \right), \text{ and} \\ S_d &= \frac{1}{\rho |\nabla Y_p|} \left( -\dot{\omega}_p - \frac{\partial}{\partial x_j} \left( \frac{\mu}{Sc} \frac{\partial Y_p}{\partial x_j} \right) \right). \end{aligned} \quad (2)$$

We denote the overall velocity of the edge point  $\mathbf{V}_e$  and break this down in the orthonormal coordinates  $\mathbf{N}_Z$  and  $\mathbf{T}_2$  as:

$$\mathbf{V}_e = S_Z \mathbf{N}_Z + S_e \mathbf{T}_2, \quad (3)$$

where  $S_e = \mathbf{V}_e \cdot \mathbf{T}_2$  is the projection of  $\mathbf{V}_e$  into in the plane of the mixture-fraction iso-surface and needs to be determined. By taking the dot product of equation 3 with  $\mathbf{N}_{Y_p}$ , it is can be shown that

$$S_e = \frac{S_d - k S_Z}{\sqrt{1 - k^2}}, \quad (4)$$

where  $k$  is the inner product of the normal vectors  $\mathbf{N}_{Y_p} \cdot \mathbf{N}_Z$ .

Although the presentation here is slightly different, it can be verified that the final result is the same edge speed used first by Pantano (2004) to study extinction holes, and later by Hawkes *et al.* (2007) to study extinction and reignition.

To provide a better interpretation of the observed edge flame speeds, some normalisation is required. In premixed combustion, where  $S_d$  is the relevant speed, a density-weighted normalisation is often applied to correct for expansion across the flame as

$$S_d^*/S_L = \frac{\rho S_d}{\rho_u S_L}, \quad (5)$$

where  $\rho_u$  is the unburned gas density and  $S_L$  is the laminar flame speed. This is equivalent to normalising by the  $S_d$  value at the  $Y_p = Y_p^*$  iso-surface in the unstrained 1D laminar flame, which we denote  $S_{d,L}$ . In the case of an edge flame, the normalisation is less straightforward because the expansion across the flame is less than  $\rho_u/\rho$  due to streamline divergence around the edge flame. However, there does not seem to be a straightforward way to define an appropriate density correction because the amount of streamline divergence is dependent on the upstream mixture-fraction gradient. Therefore, following previous studies of edge flames (Echekki & Chen, 1998; Im & Chen, 2001; Hawkes *et al.*, 2007), we simply adopt the same normalisation as used in premixed combustion to normalise all of the relevant speeds, i.e.:

$$\frac{S_e^*}{S_L} = \frac{S_e}{S_{d,L}}, \text{ and } \frac{S_Z^*}{S_L} = \frac{S_Z}{S_{d,L}}. \quad (6)$$

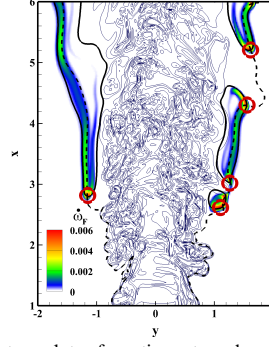


Figure 3: Contour plots of reaction rate and vorticity on the plane  $z = 0$ . The solid black line is the product mass fraction,  $Y_p$ , of 0.2 and the dashed black line is the mixture-fraction,  $Z$ , of 0.07. The identified flame edges are marked as the centres of the red circles.

To investigate the contribution of different terms in equations 3, the normalised displacement speeds are decomposed as (Echekki & Chen, 1998),

$$\begin{aligned} S_{d,n}^* &= \frac{\mathbf{N}_{Y_p} \cdot \nabla (\rho D \mathbf{N}_{Y_p} \cdot \nabla Y_p)}{\rho |\nabla Y_p|}, \\ S_{d,t}^* &= -\frac{\mu}{Sc} \frac{\kappa_{Y_p,m}}{\rho}, S_{d,r}^* = \frac{\dot{\omega}_p}{\rho |\nabla Y_p|}, \\ S_{Z,n}^* &= -\frac{\mathbf{N}_Z \cdot \nabla (\rho D \mathbf{N}_Z \cdot \nabla Z)}{\rho |\nabla Z|}, \text{ and } S_{Z,t}^* = -\frac{\mu}{Sc} \frac{\kappa_{Z,m}}{\rho}, \end{aligned} \quad (7)$$

where  $\kappa_{Y_p}$  is the curvature of the product mass fraction iso-surface defined as  $\nabla \cdot \mathbf{N}_{Y_p}$  and  $\kappa_Z$  is the mixture-fraction surface curvature defined as  $\nabla \cdot \mathbf{N}_Z$ . The subscript  $n$ ,  $t$  and  $r$  represent the components resulting from diffusion normal to product mass fraction iso-surfaces, diffusion tangential to product mass-fraction iso-surfaces, and reaction terms, respectively.

## EDGE-VELOCITY STATISTICS

In this section, the statistics of quantities obtained at all identified edge-flame locations are considered to learn how the speeds and orientations depend upon the scalar dissipation rate, in order to understand the overall dynamics.

Following earlier studies of extinction and reignition (Pantano (2004); Hawkes *et al.* (2007)), we therefore select a edge-flame marker that is the intersection of a mixture-fraction iso-surface and a product mass-fraction iso-surface.

To select the mixture-fraction iso-value, it was first assumed that the leading edge would be found at the mixture fraction having the highest laminar flame speed,  $Z_{ms}$ , which is slightly rich of stoichiometric (0.07 in this study, i.e.  $1.2 Z_{st}$ ). To select the product mass-fraction iso-surface, a one-dimensional (1D) simulation of a laminar premixed flame having the same flame parameters as the turbulent lifted flame was performed. The product mass fraction corresponding to the location of maximum heat release rate was obtained from this simulation. The obtained value of  $Y_p$  was 0.2.

For orientation, figure 3 shows an instantaneous contour plot of reaction rate and vorticity at the  $z = 0$  plane. The solid line shows the line of constant product mass fraction  $Y_p = 0.2$  and the dashed line represents the mixture fraction equal to 0.07. The identified flame edges are marked as the centres of the red circles. It may be observed that the identified flame edges correspond well with regions of high reaction rate at the leading edge as well as at flame holes observed downstream.

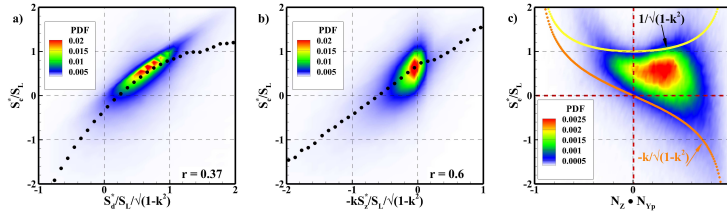


Figure 4: Contours of joint PDFs of  $S_e^*/S_L$  with a) the contribution to  $S_e^*/S_L$  of the normalised product mass-fraction displacement speed ( $S_d^*/S_L/\sqrt{1-k^2}$ ), b) the contribution to  $S_e^*/S_L$  of the normalised mixture-fraction displacement speed ( $-kS_z^*/S_L/\sqrt{1-k^2}$ ), and c) the inner product  $k$  of the normal vectors to product mass-fraction and mixture-fraction iso-surfaces.

## CONTRIBUTION OF DIFFERENT TERMS IN EDGE-FLAME PROPAGATION VELOCITY

The statistics of  $S_e^*$ , i.e. the edge-flame displacement speed along the mixture-fraction iso-surface towards reactants, are first investigated by looking into the correlations from its contributors, namely the term involving the displacement speed of product mass-fraction iso-surfaces,  $S_d^*/S_L/\sqrt{1-k^2}$ , and the term involving the displacement speed of the mixture-fraction iso-surfaces,  $-k^*S_z^*/S_L/\sqrt{1-k^2}$ . The effect of the normal vector alignment, measured by  $k = \mathbf{N}_Z \bullet \mathbf{N}_{Y_p}$ , is also considered.

Figure 4(a) shows the joint PDF of  $S_e^*/S_L$  and  $S_d^*/S_L/\sqrt{1-k^2}$ , whereas figure 4(b) shows the joint PDF of  $S_e^*/S_L$  and  $-kS_z^*/S_L/\sqrt{1-k^2}$ . In both figures, the conditional mean of the ordinate on the abscissa is also shown as a black line. Such conditional means will be shown throughout the article, but for brevity the fact that these lines represent the conditional means will not be mentioned henceforth. As shown in figure 4(a), the contribution of the product mass-fraction displacement speed is positive on average, although negative values are sometimes observed. The joint PDF is narrow and aligned with the conditional mean of  $S_e^*/S_L$ .

In contrast, figure 4(b) shows that the term  $-kS_z^*/S_L/\sqrt{1-k^2}$  is generally negative. The joint PDF shows a broader region around the conditional mean value compared with figure 4(a). A positive correlation between  $S_e^*/S_L$  and both terms is observed.

Figure 4(c) shows the joint PDF of  $S_e^*$  and the inner product of the unit vectors normal to the mixture-fraction and product mass-fraction iso-surfaces,  $k$ . The yellow and orange dots show the terms  $1/S_L/\sqrt{1-k^2}$  and  $-k/S_L/\sqrt{1-k^2}$  which appear as coefficients of  $S_d^*$  and  $S_z^*$  in equation 4. It is observed that the joint PDF of  $S_e^*$  and  $k$  generally lies between the orange and yellow curves. The significance of the black curve is that it is the expected behaviour if  $S_d^*/S_L$  is order of unity and  $S_z^*/S_L \approx 0$ . The latter curve is the expected behaviour in the opposite situation ( $S_d^*/S_L \approx 0$  and  $S_z^*/S_L \approx 1$ ). This latter situation is artificial, but it does seem to bound the likely regions quite well, perhaps coincidentally.

The most likely value of  $k = \mathbf{N}_Z \bullet \mathbf{N}_{Y_p}$  is positive, but significantly smaller than unity, i.e. the vectors are somewhat but not fully aligned. Figure 4(c) shows that a positive inner-product is more probable.

## RESPONSES TO SCALAR DISSIPATION RATE

It has been suggested that scalar dissipation contributes to the stabilisation mechanism of non-premixed flames (Nazarian *et al.*, 1988; Noda *et al.*, 2005). Therefore, in this section the effect of scalar dissipation rate on the edge-flame displacement speeds and orientations will be discussed.

Figure 5(a) shows the joint PDF of  $S_e^*/S_L$  and logarithm of the normalised scalar dissipation rate and its con-

ditional mean. The joint PDF shows a predominant negative correlation consistent with expectations from theory (Buckmaster, 2002; Ghosal & Vervisch, 2000) and the previous DNS study of Pantano (2004). The most probable  $S_e^*$  is approximately  $0.6S_L$ . A sudden drop of  $S_e^*$ , leading to negative values (i.e. local extinctions), may be observed in figure 5(a) to occur around  $\chi S_L/\delta_L \approx 1$ , as may be expected.

Figures 5(b) and (c) show the joint PDFs of  $S_d^*/S_L$  (b) and  $S_z^*/S_L$  (c) with scalar dissipation rate. It is noted that both PDFs are broad. A negative correlation with scalar dissipation rate is exhibited by  $S_d^*/S_L$ , as expected, whereas  $S_z^*/S_L$  exhibits a positive correlation.

The joint PDF of the inner-product of the normal vectors,  $k$ , is shown in figure 5(d). A clear correlation is observed, with low levels of alignment more likely at lower dissipation rate, and higher levels of alignment more likely at higher dissipation rates. This of course affects the joint PDFs of the orientation coefficients for  $S_d^*/S_L$  and  $S_z^*/S_L$  in equation 4 with scalar dissipation rate. Such alignment is expected, because high dissipation rates are the result of persistent straining, which also tends to align scalar gradients, as noted in early studies of passive scalar mixing, for example the study by Juneja & Pope (1996).

Synthesising the picture from figures 5(a)–(d),  $S_d^*$  plays the main role in the scalar dissipation rate response for moderate dissipation rates. The mixture-fraction iso-surface displacement speeds are not insignificant for moderate scalar dissipation rates. However, at large dissipation rates, the normal vectors tend to become aligned, which steepens the response of the  $S_d^*$ -related term, and results in a large contribution from  $S_z^*$  to significantly increase the negative correlation with scalar dissipation rate, thus leading to more rapid extinction.

To further understand the response of  $S_d^*$  to scalar dissipation,  $S_d^*$  is broken down into components representing the effects of reaction, normal and tangential diffusion (Eckekki & Chen, 1998) – see equation 8.

The joint PDFs of the reaction, tangential and normal diffusion components of  $S_d^*$  with scalar dissipation rate are presented in figure 6. It may be observed that the reaction term features a strong positive correlation with scalar dissipation rate whereas the tangential diffusion term exhibits a strong negative correlation. Figure 6(c) shows a weaker non-monotonic contribution of the normal diffusion term, especially at moderate dissipation rates, and also a narrow PDF around the conditional mean. Comparison of figures 5(d) and 6 suggests that the positive correlation of the reaction term with scalar dissipation rate must be dominated by the negative correlation of the tangential diffusion term for moderate scalar dissipation rates, with the normal diffusion term playing a role at larger dissipation rates.

The reason behind these correlations is now investigated. We first note that because the edge-flames are located at fixed product mass-fraction and mixture-fraction

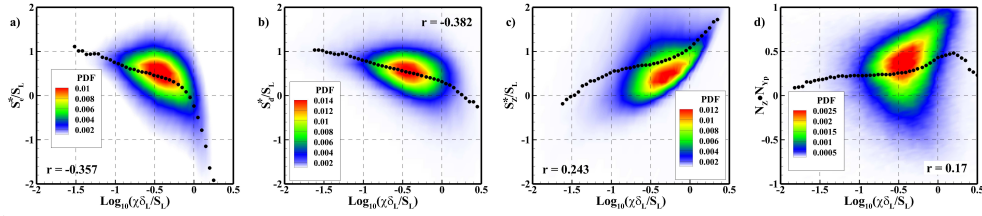


Figure 5: The joint PDFs with logarithm of the normalised scalar dissipation rate of the following quantities and their conditional means: a)  $S_e^*/S_L$ , b)  $S_d^*/S_L$ , c)  $S_z^*/S_L$ , d) the inner product of the normal vectors,  $k$ .

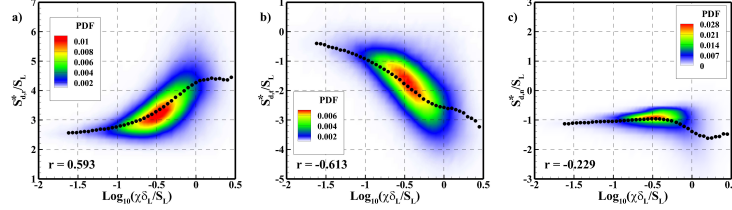


Figure 6: The joint PDFs of the components of the product mass-fraction propagation velocity a)  $S_{d,r}^*/S_L$ , b)  $S_{d,t}^*/S_L$  and c)  $S_{d,n}^*/S_L$  with the logarithm of normalised scalar dissipation rate.

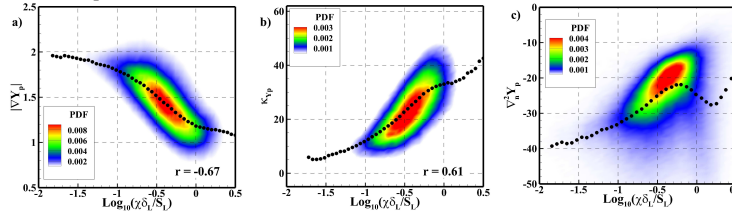


Figure 7: Contours of the joint PDFs with normalised scalar dissipation rate of: a) the magnitude of the product mass-fraction gradient, b) the product mass-fraction curvature, and c) the second derivative of the product mass fraction in the normal direction.

iso-surfaces, the reaction rate itself only experiences small fluctuations due to compressibility effects. It can therefore be taken as a constant in this discussion. The reaction term is then simply proportional to the reciprocal of the magnitude of the product mass-fraction gradient,  $1/|\nabla Y_p|$ , which scales with the thermal thickness. The normal diffusion term is approximately proportional to the second derivative of mass fraction in the normal direction  $-\nabla_n^2 Y_p/|\nabla Y_p|$  and the tangential term is curvature dependent. Figure 7(a) presents the joint PDF of  $|\nabla Y_p|$  and scalar dissipation rate where a negative correlation of  $|\nabla Y_p|$  and scalar dissipation rate may be observed. This can easily be understood in terms of the PDF of  $k$ , which shows that on average the normal vectors are not strongly aligned, and often close to perpendicular, implying that a compressive strain for mixture-fraction iso-surfaces, leading to high dissipation rates, corresponds more often to an extensive strain on product mass-fraction iso-surfaces. This correlation in turn leads to a positive correlation of the reaction term and scalar dissipation term (figure 6(a)).

As shown in equation 8, the tangential diffusion term is proportional to the curvature of the product mass-fraction iso-surfaces. Figure 6(b) therefore suggests that there is an underlying correlation between the curvature and scalar dissipation rate. To confirm this, figure 7(b) shows the joint PDF of  $\kappa_p$  and  $\log_{10}(\chi\delta_L/S_L)$ . A strong positive correlation is observed as expected. Similarly to the above discussion, this may be explained considering the earlier result for the alignment of the normal vectors, shown in figure 4(c), which demonstrated that the most likely inner product of the normal vectors was significantly smaller than unity. In this situation, compressive strain in the direction of the mixture-fraction normal, which leads to high dissipation rates, causes increases of the product mass fraction curvature.

To explain the trends for the normal diffusion compo-

nent, figure 7(c) shows the joint PDF of  $\nabla_n^2 Y_p$  and  $\chi$ . As may be observed,  $\nabla_n^2 Y_p$  is negatively correlated in magnitude with scalar dissipation rate, but this is offset by a positive correlation between scalar dissipation rate and  $1/|\nabla Y_p|$ , which can be inferred from figure 7(a). For moderate dissipation rates, the correlation with  $\nabla_n^2 Y_p$  is dominant, leading to a positive correlation for  $S_n^*/S_L$  with scalar dissipation rate. In contrast, for larger dissipation rates ( $\log_{10}(\chi\delta_L/S_L) > -0.5$ ), the correlation with  $1/|\nabla Y_p|$  dominates, leading to a negative correlation for  $S_n^*/S_L$  with scalar dissipation rate.

We now investigate the behaviour of  $S_z^*$  components. The joint PDFs of normal diffusion term in figure 8(a) shows a positive correlation with scalar dissipation rate whereas a negative correlation is observed for the joint PDFs of tangential diffusion term in figure 8(b). The normal diffusion term is dominant, explaining the positive correlation of  $S_z^*$  with scalar dissipation rate that was observed in figure 5(e).

The normal diffusion component is approximately proportional to  $\nabla_n^2 Z/|\nabla Z|$ . Figure 8(c) shows that  $\nabla_n^2 Z$  varies approximately quadratically with  $|\nabla Z|$ , which can be understood with the scalings  $\nabla_n^2 Z \approx 1/\delta_Z^2$  and  $|\nabla Z| \approx 1/\delta_Z$ , where  $\delta_Z$  is a diffusive length scale. This explains the positive correlation observed between  $S_{z,n}^*$  and the scalar dissipation rate (figure 6(c)).

To explain the relatively weaker positive correlation between  $S_{z,t}^*$  and scalar dissipation rate, figure 8(d) shows the joint PDF of  $\kappa_z$  and scalar dissipation rate. In the region that contains most of the sample, the correlation is positive. Extensive visual inspections of three-dimensional renderings of mixture-fraction iso-surfaces coloured by dissipation rate (not shown) suggest that this positive correlation results from specific eddy structures in the jet. The highest dissipation rates are observed to occur in structures which bulge out towards the oxidiser side, thus having a positive

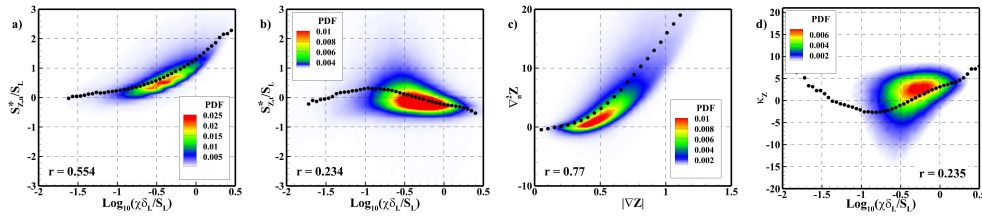


Figure 8: The joint PDFs of the components of the mixture-fraction propagation velocity a)  $S_{Z,n}^e$ , b)  $S_{Z,t}^e$  with the logarithm of normalised scalar dissipation rate, c) Laplacian of mixture-fraction normal to mixture-fraction iso-surface with mixture-fraction gradient; and d) the joint PDF of the mixture-fraction curvature and the scalar dissipation rate.

mixture-fraction curvature. As discussed above, higher gradients correspond to an even higher normal second derivative, which leads to the increase in the normal diffusion component of  $S_Z^e$  with scalar dissipation rate.

## CONCLUSION

The edge-flame concept received a great deal of attention in last couple of years in terms of its potential role in stabilisation process of turbulent lifted flames. In the present work, DNS (Karami *et al.*, 2014) was used to analyse the edge flame and flow interactions. The product mass fraction contribution in the edge-flame velocity is mainly positive while the mixture fraction propagation velocity has a negative contribution. The normal vectors were somewhat but not fully aligned. The edge-flame velocity decays as scalar dissipation increases and a sudden drop occurs at scalar dissipation in order of reciprocal of the laminar flame time scale. This sudden drop to a negative value, which may be interpreted as extinction, is mainly due to the mixture fraction propagation velocity contribution, which becomes significant because of high levels of gradient alignment.

It was found that the negative correlation of the product mass fraction propagation velocity with scalar dissipation is mainly caused by the tangential and diffusion terms whose its negative correlation with scalar dissipation overtakes the competing positive correlation of the reaction term with scalar dissipation rate. The tangential term in the product mass fraction velocity is product mass fraction curvature dependent and this curvature shows a positive correlation with the scalar dissipation rate. The reaction term correlation with the scalar dissipation depends on the product mass fraction gradient. The positive correlation of the mixture fraction propagation velocity with scalar dissipation rate was shown to be mainly due to the positive response of normal term to increase in scalar dissipation rate as this increase leads to a decrease in diffusive length scale and correspondingly increase in diffusion term.

## ACKNOWLEDGEMENT

This work was supported by the Australian Research Council. The research benefited from computational resources provided through the National Computational Merit Allocation Scheme, supported by the Australian Government. The computational facilities supporting this project included the Australian NCI National Facility, the partner share of the NCI facility provided by Intersect Australia Pty Ltd., the Peak Computing Facility of the Victorian Life Sciences Computation Initiative (VLSCI), iVEC (Western Australia), and the UNSW Faculty of Engineering.

## REFERENCES

Arndt, C. M., Schiel, R., Gounder, J. D., Meier, W. & Aigner, M. 2013 *Proc. Combust. Inst.* **34** (1), 1483 – 1490.  
 Buckmaster, J. 2002 *Prog. Energy Combust. Sci.* **28** (5), 435–475.

Chakraborty, N. & Cant, S. 2004 *Combust. Flame* **137** (1), 129–147.  
 Chen, J. H., Choudhary, A., De Supinski, B., Devries, M., Hawkes, E. R., Klasky, S., Liao, W. K., Ma, K. L., Mellor-Crummey, J., Podhorszki, N., Sankaran, R., Shende, S. & Yoo, C. S. 2009 *Comput. Sci. Disc.* **2** (1).  
 Chung, S. H. 2007 *Proc. Combust. Inst.* **31** (1), 877 – 892.  
 Echekki, T. & Chen, J. H. 1998 *Combust. Flame* **114** (12), 231 – 245.  
 Fernández-Tarrazo, E., Sánchez, A. L., Liñán, A. & Williams, F. A. 2006 *Combust. Flame* **147** (12), 32 – 38.  
 Garrido-López, D. & Sarkar, S. 2005 *Proc. Combust. Inst.* **30** (1), 621 – 628.  
 Ghosal, S. & Vervisch, L. 2000 *J. Fluid Mech.* **415**, 227–260.  
 Gordon, R. L., Boxx, I., Carter, C., Dreizler, A. & Meier, W. 2012 *Flow Turbul. Combust.* **88** (4), 503–527.  
 Hawkes, E. R. & Chen, J. H. 2006 *Combust. Flame* **144** (1), 112–125.  
 Hawkes, E. R., Sankaran, R. & Chen, J. H. 2007 Reignition dynamics in massively parallel direct numerical simulations of COH<sub>2</sub> jet flames. pp. 1271–1274. 16th Australasian Fluid Mechanics Conference.  
 Im, H. G. & Chen, J. H. 2001 *Combust. Flame* **126** (1), 1384–1392.  
 Juneja, A. & Pope, S. B. 1996 *Phys. Fluids* **8** (8), 2161–2184.  
 Karami, S., Hawkes, E. R. & Talei, M. 2012 A direct numerical simulation study of a turbulent lifted flame in hot oxidizer. p. 149. 18th Australasian Fluid Mechanics Conference.  
 Karami, S., Hawkes, E. R., Talei, M. & Chen, J. H. 2014 *J. Fluid Mech.* **Submitted**.  
 Karami, S., Hawkes, E. R., Talei, M. & Chen, J. H. 2015 Edge flame dynamics in a turbulent lifted jet flame. pp. 137–146. Proceedings of the 2014 CTR Summer Program.  
 Namazian, M., Schefer, R. W. & Kelly, J. 1988 *Combust. Flame* **74** (2), 147–160.  
 Noda, S., Mori, H., Hongo, Y. & Nishioka, M. 2005 *JSME Int. J. B-Fluid T* **48** (1), 75–82.  
 Pantano, C. 2004 *J. Fluid Mech.* **514**, 231–270.  
 Passot, T. & Pouquet, A. 1987 *J. Fluid Mech.* **181**, 441–466.  
 Phillips, H. 1965 *Symp. (Int.) Combust.* **10** (1), 1277–1283.  
 Pope, S. B. 1988 *Int. J. Eng. Sci.* **26** (5), 445–469.  
 Stärner, S. H., Bilger, R. W., Frank, J. H., Marran, D. F. & Long, M. B. 1996 *Combust. Flame* **107** (3), 307 – 313.  
 Su, L. K., Sun, O. S & Mungal, M. G 2006 *Combust. Flame* **144** (3), 494–512.  
 Upatnieks, A., Driscoll, J. F., Rasmussen, C. C. & Ceccio, S. L. 2004 *Combust. Flame* **138** (3), 259 – 272.  
 Yoo, C. S., Sankaran, R. & Chen, J. H. 2009 *J. Fluid Mech.* **640**, 453–481.